A tiny lensless position sensing device for the tracking of active markers

Thibaut Raharijaona, Paul Mignon, Raphaël Juston, Stéphane Viollet

A tiny lensless position sensing device for the tracking of active markers

T. Raharijaona *, **P. Mignon** *, **R. Juston** * **and S. Viollet** *

* *Aix-Marseille Université, CNRS, ISM UMR 7287, 13288, Marseille cedex 09, France*

Abstract: Active markers tracking is performed using an innovative insect-based visual sensor. Without any optics and a field-of-view of about 60°, our novel miniature visual sensor is able to locate flickering markers (LEDs) with accuracy much greater than the one dictated by the pixel pitch. With a size of only $1cm^3$ and a mass of only 0.33g, the lensless sensor, called HyperCube, is dedicated to 3D motion tracking and fits perfectly with the drastic constraints imposed by micro-aerial vehicles. This small cubic position sensing device is composed of only three photosensors placed on each side of the cube, making this sensor very cheap and light. HyperCube provides the azimuth and elevation of infrared LEDs flickering at high frequency (>1kHz) with a precision of only few degrees. The simplicity, small size, low mass, and low power consumption of this optical sensor make it suitable for many applications in the field of cooperative flight of unmanned aerial vehicles, swarm robotics and more generally robotic applications requiring active beacons. Experimental results show that HyperCube provides useful angular measurements that can be used to estimate the relative position between the sensor and the infrared markers.

Keywords: Sensors, Visual motion, Tracking applications, Robotics, View angles.

1. INTRODUCTION

The recent development of sensing devices embedded onboard micro-aerial vehicles (MAVs) has required the design of very light weight and miniature sensors. A main challenge relies on the development of advanced miniature sensors that can substitute for classical devices such as bulky stereoscopic cameras Audette et al. (2000) or ultrasonic sensors Cardin et al. (2006). Recently, a novel class of optical sensors has been introduced for aerospace applications. For instance, new flexible compound-eyes have been proposed for motion extraction and proximity estimation based on optic flow principle Dobrzynski et al. (2012); Floreano et al. (2013). Furthermore, proximity sensor has also been presented in Roberts et al. (2012); Wenzel et al. (2012). These studies depict embedded infrared (IR) based 3-D relative positioning sensor dedicated to inter-robot spatial-coordination and cooperative flight. Dealing with the ability to determine the spatial orientation and placement of the unmanned aerial platform in real time, the cooperative flight tends to incorporate leader-follower UAVs using vision processing, radio-frequency data transmission and more sensors. Then, the cooperative flight requires the control of only one UAV and should allow the deployment of multiple UAVs. Etter et al. (2011) have designed and evaluated a leader-follower autonomous aerial quadrotor system for search and rescue operations using an IR camera and multiple IR beacons. Masselli and Zell (2012) have proposed a novel method for pose estimation for micro aerial vehicles using passive visual markers and a monocular color camera mounted onto the MAV as the only sensor.

⋆ e-mail: {thibaut.raharijaona,raphael.juston,stephane.viollet}@univ-amu.fr,paul.mignon@phelma.grenoble-inp.fr

In this paper, we present a novel optical sensor, called HyperCube, endowed with hyperacuity Westheimer (1981) for active IR LED markers tracking applications. The principle, on which HyperCube is based, was developed by Kerhuel et al. and detailed in Kerhuel et al. (2012) and Juston et al. (2013). The markers we used are off-the-shelf IR LEDs flickering at high frequency (>1kHz). We envision that this sensor could be used for cooperative flight as presented in Fig 1.

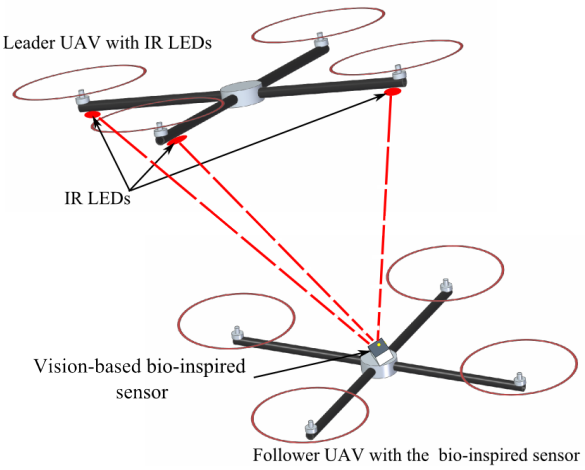

Fig. 1. Sketch of a collaborative flight using IR LEDs and the HyperCube sensor embedded onboard the follower.

The purpose of this paper is to show the promising features of HyperCube in terms of azimuth and elevation measurements of a pattern (planar object) composed of flickering IR LEDs. We also show the abilities of HyperCube to measure its relative position with respect to the markers.

The paper is organized as follows: Sec. 2 details the principle of the sensor, the visual processing algorithm and its advantages. The principle of the sensor is discussed in Sec. 3. The experimental setup is presented in Sec. 4 and Sec. 5 shows experimental results.

2. MODELING THE HYPERCUBE SENSOR

The prototype was built using off-the-shelf elements. Its volume is $1cm^3$ and it weights 0.33g. These characteristics make it cheap, light, tiny and power-lean.

2.1 Angular sensitivity of the photosensors

The HyperCube sensor is composed of three surface mounted device (SMD) photodiodes (VISHAY TEMD7000). Each photodiode (or photosensor) is located on each side of the cube as shown in Fig 2A. Thanks to this cubic assembly, the optical axes of each pair of photosensors are separated by an angle of 90°. On each side of the sensor, an analog circuit (Fig. 2B) converts the ouput current of the photodiode into a proportional voltage.

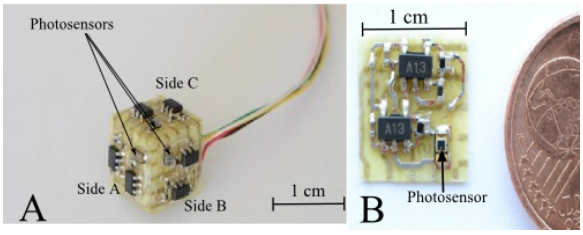

Fig. 2. A. Each side of the HyperCube sensor integrates one photosensor and an analog amplifier for the conversion of the photodiode current into an output voltage.
B. One side of the HyperCube sensor with one photosensor (tiny SMD photodiode).

HyperCube can extract two angular positions (azimuth and elevation) from the position of a pattern composed of several IR LEDs. The IR LEDs used in the experimental setup are the OSRAM SFH4232. Their spectrum have a maximum emissive power at a wavelength of 900nm which corresponds to the maximum of absorption of the photosensors. Thereafter, the IR LEDs will be considered as a point. The signal processing used to estimate the elevation and azimuthal angles from the three HyperCube output signals runs in real time onboard a custom-made electronic board described in Sec. 2.2.

2.2 Model of the photosensor output signal

The cosine-like angular sensitivity function for each photosensor depends on the azimuth and elevation as shown in Fig. 3. It mimicks the Gaussian angular sensitivity function of flies' photoreceptors Götz (1964).

Each IR LED signal is modulated at a specific frequency f_i. The modulation is provided by a custom-made electronic board (Fig. 4A). The latter was designed to provide one specific modulation frequency f_i to each LED such that $f_1 = 1$kHz, $f_2 = 3.5$kHz, $f_3 = 11.5$kHz for the three separated IR LED emitters of the pattern. Then, an additional custom-made processing board (Fig. 4B) achieved the analog signal demodulation for each frequency f_i. To

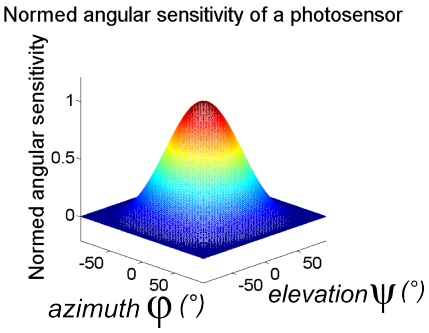

Fig. 3. Cosine-like angular sensitivity of a photosensor.

summarize, two electronic boards have been designed and realized: one board in charge of the modulation of the LEDs and a second board, connected to HyperCube, which is in charge of the analog demodulation and the digital visual processing .

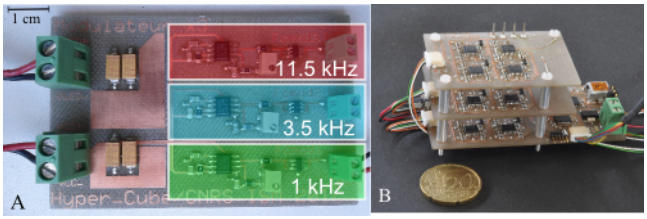

Fig. 4. A. Custom-made electronic board for the frequency modulation of the IR LEDs. It produces three separate signals that blink at 1kHz, 3.5kHz and 11.5kHz sent to the three IR LEDs of the pattern to be located.
B. Custom-made acquisition and demodulation board. It is composed of three analog demodulation circuits. A microcontroller processes the visual output signal yielded by HyperCube and provides the azimuth and the elevation which are sent through a USB interface to a PC.

Once the three HyperCube output signals are demodulated, amplified and filtered by a low-pass filter at 100Hz, one can approximate for each photosensor Ph_i and frequency f_i, the output signal S_{Ph_i,f_i} of HyperCube. We introduce the angular sensitivity function σ such that:

$$\sigma(\theta) = \begin{cases} \frac{1}{2}(cos(2\theta)+1) & if\ |\theta| \leq 90° \\ 0 & else \end{cases}$$

Therefore, S_{Ph_i,f_i} is defined as follows:

$$S_{Ph_1,f_i}(\varphi,\psi) = A_{1,i}\sigma(\varphi - 45°).\sigma(\psi + 45°)$$
$$\text{if } |\varphi - 45°| < 90° \text{ and } |\psi + 45°| < 90° \text{ else } S_{Ph_1,f_i}(\varphi,\psi) = 0$$

$$S_{Ph_2,f_i}(\varphi,\psi) = A_{2,j}\sigma(\varphi + 45°).\sigma(\psi + 45°)$$
$$\text{if } |\varphi + 45°| < 90° \text{ and } |\psi + 45°| < 90° \text{ else } S_{Ph_2,f_i}(\varphi,\psi) = 0$$

$$S_{Ph_3,f_i}(\varphi,\psi) = A_{3,j}\sigma(\varphi).\sigma(\psi - 45°)$$
$$\text{if } |\varphi| < 90° \text{ and } |\psi - 45°| < 90° \text{ else } S_{Ph_3,f_i}(\varphi,\psi) = 0$$

with $A_{1,i}$, $A_{2,i}$, $A_{3,i}$, the gains of the photosensors Ph_1, Ph_2 or Ph_3 on each side of the HyperCube sensor. The indice i refers to the frequencies 1kHz, 3.5kHz, 11.5kHz. φ and ψ are the azimuth and elevation with respect to the IR LED$_i$.

The three photosensor (photodiode) output signals are processed by a microcontroller dsPIC 33FJ128GP802. As shown in Fig. 5A and B, the digital processing operates at

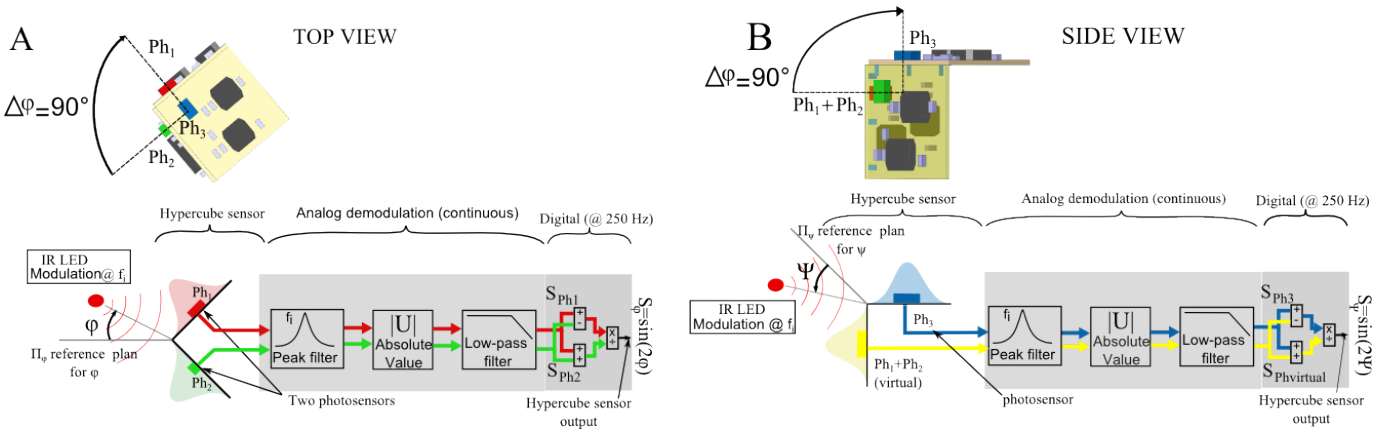

Fig. 5. Sketch diagram of HyperCube signal processing algorithm.

A. Top view: the sensor measures the azimuth φ. The left part shows the IR LED modulated at a frequency noted f_i (1kHz, 3.5kHz or 11.5kHz). In this view, HyperCube is composed of two photosensors Ph_1 and Ph_2 with their respective cosine-like angular sensitivities corresponding to the sides A and C of the sensor (see Fig. 2A). An analog band-pass filter acts as a demodulator to extract the signal corresponding to the frequency f_i of the IR LED and an analog low-pass filter section reduces the high-frequency noise and prevents the subsequent analog-to-digital conversion from any aliasing effects. The digital processing consists in computing the ratio of relative difference to the sum between the two signals ($\frac{S_{Ph_1}-S_{Ph_2}}{S_{Ph_1}+S_{Ph_2}}$) to yield the HyperCube sensor output signal.

B. Side View: the same signal processing is applied on the signal provided by the photosensor Ph_3 (side B in Fig. 2A) of HyperCube and a virtual photosensor which is the sum of the photosensors Ph_1 and Ph_2.

250Hz and computes the relative difference over the sum of two adjacent photosensor signals.

2.3 Advantages of HyperCube

HyperCube exhibits several advantages over other conventional sensors like CMOS cameras according to these following points:

- low cost : there is no optics, the angular position measurement relies only on the angular sensitivity of photodiodes which is, by essence, non uniform (cosine law) and only requires very cheap off-the-shelf electronic components.
- low computational resource: the measurements are angular informations, it does not require any image processing. High refresh rate for the same computational resource can easily be reached.
- small size: because of a low number of components, the sensor is light weight (0.33g) and very compact ($1cm^3$).

3. PRINCIPLE OF THE HYPERCUBE SENSOR

3.1 Angle reconstruction

Let's consider the azimuth angle φ. It is defined as the angle between the reference plane Π_φ (see Fig. 6A) and a plane including the IR LED (see red dotted line in Fig. 6A). Π_φ is the midplane between the photosensors Ph_1 and Ph_2. The second plane includes the IR LED and the the intersection between the optical axes of Ph_1 and Ph_2. In Fig. 6A, the azimuth angle φ is presented in top view and in front view in Fig. 6B. The digital processing operated in the microcontroller with respect to the azimuth φ returns an output signal whose the theoretical expression can be written as :

$$S_\varphi = \frac{S_{Ph_1} - S_{Ph_2}}{S_{Ph_1} + S_{Ph_2}} \tag{1}$$

$$S_\varphi = \frac{A_1[cos(2(\varphi - 45°)) + 1] - A_2[cos(2(\varphi + 45°)) + 1]}{A_1[cos(2(\varphi - 45°)) + 1] + A_2[cos(2(\varphi + 45°)) + 1]} \tag{2}$$

$$S_\varphi = \frac{[A_1 + A_2]sin(2\varphi) + A_1 - A_2}{[A_1 - A_2]sin(2\varphi) + A_1 + A_2} \tag{3}$$

A_1 and A_2 are gains of the signals delivered by the photosensors Ph_1 and Ph_2. If we assume $A_1 = A_2$, (3) gives $S_\varphi = sin(2\varphi)$.

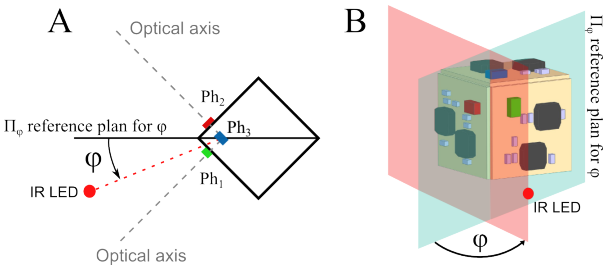

Fig. 6. Reconstruction of the azimuth φ

A. Top view with the reference plane Π_φ which is the plane through the IR LEDs and the optical axes of the photosensor Ph_1 and the photosensor Ph_2,

B. Front view which gives an illustration of the azimuth φ and the reference planes.

Let's consider the elevation angle ψ. Here, we introduce the reference plane Π_ψ (see Fig. 7). Π_ψ is orthogonal to the reference plane Π_φ. The elevation angle ψ is defined as the angle between the reference plane Π_ψ (see Fig. 7) and a plane including the IR LED (see red dotted line in Fig. 8A). The second plane includes the IR LED and the

intersection of the optical axes of the virtual photodiode $(Ph_1 + Ph_2)$ and Ph_3.

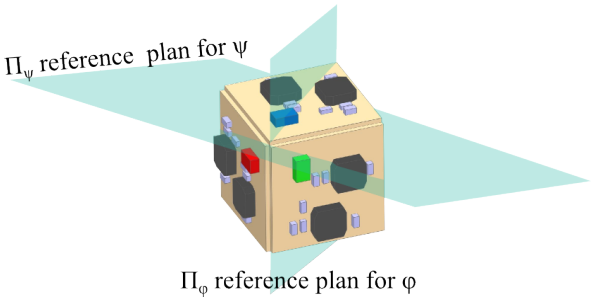

Fig. 7. Definition of the second reference plane Π_ψ in relation with the first reference plane Π_φ. Note that the plane Π_ψ is orthogonal to the plane Π_φ.

In Fig. 8A, the elevation angle is presented in side view and in front view in Fig. 8B.

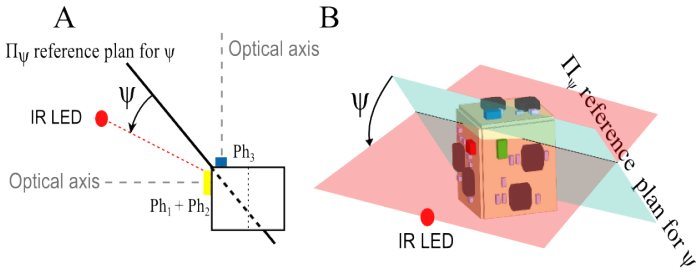

Fig. 8. Schematic of the elevation angle ψ
A. Side view with the reference plane Π_ψ which is the plane through the LED and the optical axes of the virtual photosensor $(Ph_1 + Ph_2)$ and the photosensor Ph_3
B. Front view gives an illustration of the elevation angle ψ and the reference planes.

The digital processing with respect to the elevation ψ involves a virtual photosensor (Ph_1+Ph_2) which is the combination of Ph_1 and Ph_2. In the following, we introduce the signal $S_{Ph_{virtual}}$ delivered by the virtual photosensor:

$$S_{Ph_{virtual}} = S_{Ph_1} + S_{Ph_2} = A\sigma(\psi+45°).[\sigma(\varphi+45°) + \sigma(\varphi-45°)]$$
$$= \begin{cases} A\sigma(\psi+45°) & if\ |\varphi| < 45° \\ S_{Ph_1} & if\ 45° < \varphi < 135° \\ S_{Ph_2} & if\ -135° < \varphi < -45° \\ 0 & else \end{cases}$$

Similarly to (3), if we assume the gains are such that $A_1 = A_2 = A_3 = A$, the digital signal output for the elevation angle ψ gives: $S_\psi = \frac{S_{Ph_{virtual}} - S_{Ph_3}}{S_{Ph_{virtual}} + S_{Ph_3}}$. Using the definition of $S_{Ph_{virtual}}$, on can write if $|\varphi| < 45°$:

$$S_\psi = \frac{\sigma(\psi+45°) - \sigma(\varphi).\sigma(\psi-45°)}{\sigma(\psi+45°) + \sigma(\varphi).\sigma(\psi-45°)}$$

Considering the approximation of small angles for φ, $\sigma(\varphi) \simeq 1$ and one can simplify:

$$S_\psi \simeq \frac{\sigma(\psi+45°) - \sigma(\psi-45°)}{\sigma(\psi+45°) + \sigma(\psi-45°)} = \frac{[cos(2(\psi+45°))+1] - [cos(2(\psi-45°))+1]}{[cos(2(\psi+45°))+1] + [cos(2(\psi-45°))+1]}$$

Therefore,

$$S_\psi \simeq sin(2\psi)$$

3.2 Position estimation

Given the signal outputs S_ψ and S_φ and one IR LED, a first step was to assess the relative position of the IR LED in the plane (X_{LED}, Y_{LED}) with respect to HyperCube. The experimental setup detailed in Sec. 4 justifies the approximation of the small angles. Therefore, one can assume that $\varphi \simeq tan(\varphi) \simeq \frac{X_{LED}}{Z_{LED}}$ for the azimuth and $\psi \simeq tan(\psi) \simeq \frac{Y_{LED}}{Z_{LED}}$ for the elevation. If Z_{LED} is *a priori* known, using only angular measurements provided by the sensor, the relative position of the IR LED can be estimated.

4. EXPERIMENTAL SETUP

In this work, we aimed at demonstrating that the estimation of the relative position of an IR LED with respect to HyperCube can be achieved by means of angular measurements. The experimental setup is composed of a motor driven XY table as shown in Fig. 9. We oriented HyperCube so that it was pointing upward. HyperCube can move along the X and Y directions thanks to two DC motors.

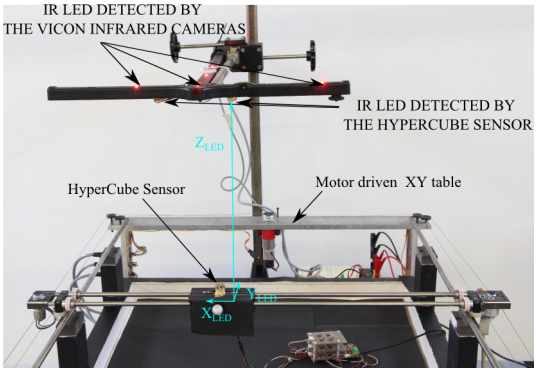

Fig. 9. XY table driven by DC motors. The the HyperCube positions is controlled in closed-loop by means of two incremental encoders. The distance Z_{LED} was assumed here to be known and constant. Additional active VICON markers were used to compare the precision of HyperCube with the ground truth acquired from the VICON motion capture system.

Two incremental encoders measure the HyperCube positions along the X and Y directions. In the initial conditions which define the origin of the inertial frame, an IR LED is located just above HyperCube at an approximate height $Z_{LED} = 300$mm. As an absolute sensor's position of reference, a tracking system called VICON was used for measuring the ground truth, i.e., the precise absolute positions of HyperCube. The tracking system is equipped with 17 IR cameras and IR active markers that are pointed upward as depicted in Fig. 9. The HyperCube position of reference was therefore measured in real time with a great precision (above one millimeter).

4.1 Position estimation

To validate the calibration for $Z_{LED} = 300\ mm$, the estimated $\hat{X}_{LED}$ and $\hat{Y}_{LED}$ of the IR LED were compared to the references X_{LED} and Y_{LED} provided by the VICON tracking system.

5. EXPERIMENTAL POSITION ESTIMATION IN 2D

In this section, we used a single IR LED and HyperCube for each experiment. We compared the estimation to HyperCube positions assessed by the tracking system for three different modulation frequencies. For the IR LED that flickers at 1kHz, Fig. 10A shows the plots of the reference trajectory in dashed line and the trajectory depicted by HyperCube in solid line.

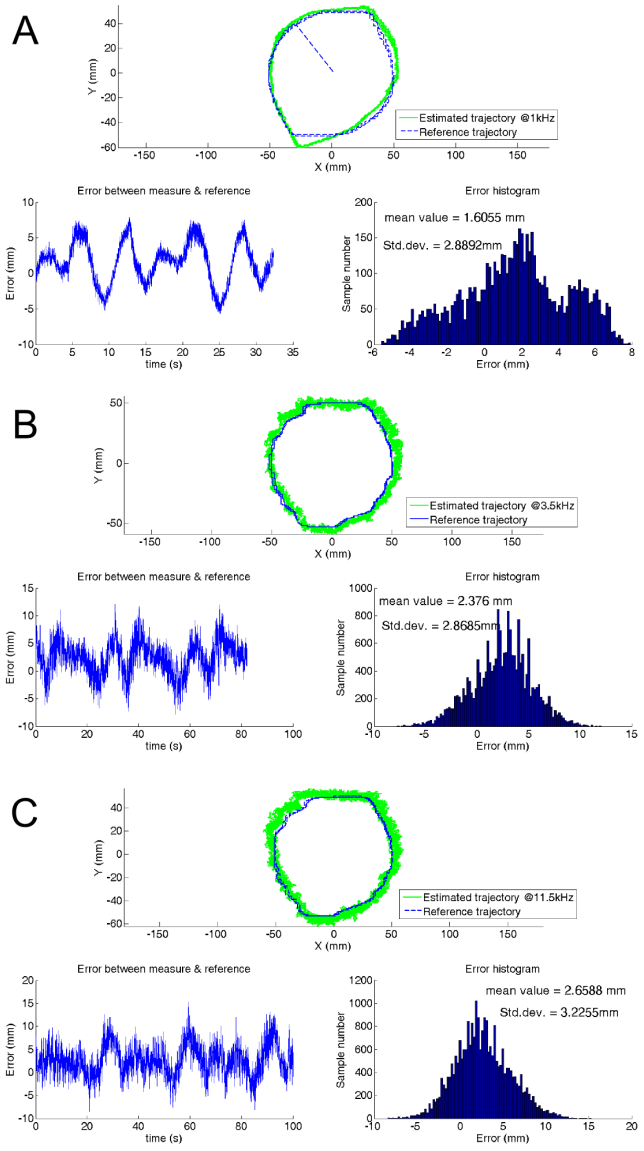

Fig. 10. A. Position estimation for a circular trajectory with a radius of 50mm in the XY plane. Note that the absolute value of the position error is lower than 10mm and that the standard deviation is about 3mm. We also note that the noise is more important for the experiments at 3.5kHz (B) and 11.5kHz (C).

The trajectory is a circular path with a radius of 50mm in the XY plane with $Z_{LED} = 300$mm. The distance between reference and estimated trajectories was also plotted. The histogram of the error gives a mean value $\mu = 1.6$mm and a standard deviation $\sigma = 2.8$mm. We noted that the noise at 1kHz for the demodulation was lower than the noise at 3.5kHz and 11.5kHz as shown in Fig. 10B and C. This can be explained by the use of different operational amplifiers (TI OPA4322 and TI OPA4342) for the analog demodulation. Figures 10A, B and C highlight that HyperCube sensor provides useful measurements to accurately estimate dynamic relative position of an IR LED in the XY plane.

In order to reduce the measurement noise, the digital signal outputs given by HyperCube sensor are fed into a linear form of a Kalman filter. As shown in Figures 11A, B and C for each frequency f_i, noise is greatly reduced.

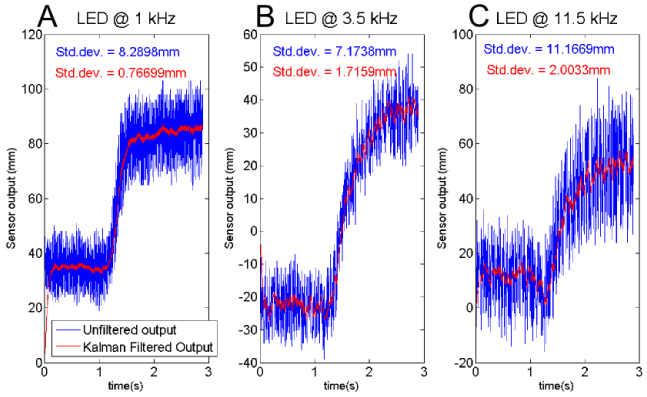

Fig. 11. Result of the Kalman filtering for the estimation of a movement in the X direction at 1kHz (A), 3.5kHz (B) and 11.5kHz (C)

5.1 IR LED position tracking in 2D

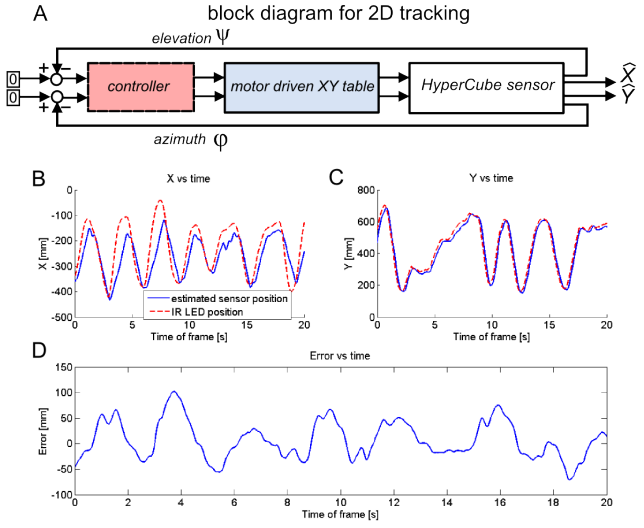

Fig. 12. Block diagram of the IR LED position tracking system characterized by moving by hand one IR LED (flickering frequency 1kHz) placed 30cm above HyperCube.
B. Experimental recording of the position tracking along the X direction versus time. The DC motor for the X axis is not powerful enough and can't follow quick variations of the reference signal.
C. Experimental recording of the position tracking along the Y direction versus time.
D. Error of the IR LED position tracking. Note that the absolute value of the position error never exceeds 10 cm.

In this section, HyperCube sensor measurements which consists in azimuth φ and elevation ψ feed the controller that aims at tracking a moving IR LED in the plane. A smith predictor with proportional and integral actions was designed and implemented to ensure a good stability of the linear displacement of HyperCube despite the time lag inherent to the visual processing algorithm.
Figure 12A shows the block diagram of the closed loop system with the assessed angles φ and ψ. In Figures 12B and C, estimated positions versus time are plotted. The tracking system gives the reference values. As shown in Fig. 12B and C, the position tracking was efficient. The error curves in the Fig 12D shows that the maximum error is lower than 10cm. Nevertheless, one can remark in Fig. 12B that there is a an error between the estimated and the reference values due to a saturation of the motor of the X axis. Thanks to a fast motor for controlling the Y axis, HyperCube was able to follow faithfully the moving pattern. In Fig. 12C, the HyperCube sensor perfectly tracks the moving IR LED. Finally, the HyperCube sensor exhibits good performances for motion tracking.

6. CONCLUSION

The HyperCube sensor is a cubic, miniature and low cost sensing device able to track active markers without any optics. It provides azimuth and elevation and is able to assess the angular position of three blinking IR LEDs at specific frequencies: 1kHz, 3.5kHz and 11.5kHz. The estimation is achieved here by a simple signal processing of the low-amplitude and high-frequency signal transmitted by the three photodiodes placed on each side of the cube. Experimental results showed that for relative position estimations, this miniature device is very efficient and features promising results in terms of distance estimation as well (not shown here). Nevertheless, the prototype developed reveals some limitations with respect to the range of pose estimation but it is well adapted for proximal localization (up to 30cm). In addition, the size of the demodulation electronic board could be easily reduced. As a conclusion, the HyperCube sensor is a promising sensing device for the localization of pattern that can be placed onboard UAVs or MAVs.

ACKNOWLEDGEMENTS

We thank M. Boyron for his assistance with the electrical design and J. Diperi for his involvement in the mechanical design of the sensor. We also thank N. Franceschini for the motor driven XY table.

REFERENCES

Audette, R., Balthazaar, J., Dunk, C., and Zelek, J. (2000). A stereo-vision system for the visually impaired. Technical Report 2000-41x-1, School of Engineering, University of Guelph, Guelph, ON, Canada.

Cardin, S., Vexo, F., and Thalmann, D. (2006). Wearable system for mobility improvement of visually impaired people. *Vis. Comp. Journal*, 23, 109–118.

Dobrzynski, M., Pericet-Camara, R., and Floreano, D. (2012). Vision tape - a flexible compound camera for motion detection and proximity estimation. *IEEE Sensors*, 1, in press. doi:10.1109/JSEN.2011.2166760.

Etter, W., Martin, P., and Mangharam, R. (2011). Cooperative flight guidance of autonomous unmanned aerial vehicles. In *The Second Int. Workshop on Networks of Cooperating Objects*.

Floreano, D., Pericet-Camara, R., Viollet, S., Ruffier, F., Brückner, A., Leitel, R., Buss, W., Menouni, M., Expert, F., Juston, R., Dobrzynski, M.K., L'Eplattenier, G., Recktenwald, F., Mallot, H.A., and Franceschini, N. (2013). Miniature curved artificial compound eyes. *Proc Natl Acad Sci U S A*, 110(23), 9267–9272. doi:10.1073/pnas.1219068110. URL `http://dx.doi.org/10.1073/pnas.1219068110`.

Götz, K. (1964). Optomotorische untersuchung des visuellen systems einiger augenmutanten der fruchtfliege *Drosophila*. *Biological Cybernetics*, 2, 77–92.

Juston, R., Kerhuel, L., Franceschini, N., and Viollet, S. (2013). Hyperacute edge and bar detection in a bioinspired optical position sensing device. *Mechatronics, IEEE/ASME Transactions on*, PP(99), 1–10. doi: 10.1109/TMECH.2013.2265983.

Kerhuel, L., Viollet, S., and Franceschini, N. (2012). The vodka sensor: A bio-inspired hyperacute optical position sensing device. *IEEE Sensors Journal*, 12(2), 315–324. doi:10.1109/JSEN.2011.2129505.

Masselli, A. and Zell, A. (2012). A novel marker based tracking method for position and attitude control of mavs. In *Proceedings of International Micro Air Vehicle Conference and Flight Competition (IMAV)*.

Roberts, J., Stirling, T., Zufferey, J.C., and Floreano, D. (2012). 3-d relative positioning sensor for indoor flying robots. *Autonomous Robots*, 33(1-2), 5–20. doi:10.1007/s10514-012-9277-0. URL `http://dx.doi.org/10.1007/s10514-012-9277-0`.

Wenzel, K., Masselli, A., and Zell, A. (2012). Visual tracking and following of a quadrocopter by another quadrocopter. In *Intelligent Robots and Systems (IROS), 2012 IEEE/RSJ International Conference on*, 4993–4998. doi:10.1109/IROS.2012.6385635.

Westheimer, G. (1981). *Visual hyperacuity*. Ottoson, Sensory Physiology 1, Springer, Berlin.